International Journal of Minerals, Metallurgy and Materials
Volume 28, Number 4, April 2021, Page 688
https://doi.org/10.1007/s12613-020-2139-4

Effect of thermomechanical cyclic quenching and tempering treatments on microstructure, mechanical and electrochemical properties of AISI 1345 steel

Muhammad Arslan Hafeez[1)], *Ameeq Farooq*[2)], *Kaab Bin Tayyab*[2)], *and Muhammad Adnan Arshad*[2)]

1) School of Civil and Environmental Engineering, National University of Sciences and Technology, Islamabad 44000, Pakistan
2) Department of Metallurgy & Materials Engineering, University of the Punjab, 54590 Lahore, Pakistan
(Received: 2 June 2020; revised: 8 July 2020; accepted: 10 July 2020)

Abstract: Thermomechanical cyclic quenching and tempering (TMCT) can strengthen steels through a grain size reduction mechanism. The effect of TMCT on microstructure, mechanical, and electrochemical properties of AISI 1345 steel was investigated. Steel samples heated to 1050°C, rolled, quenched to room temperature, and subjected to various cyclic quenching and tempering heat treatments were named TMCT-1, TMCT-2, and TMCT-3 samples, respectively. Microstructure analysis revealed that microstructures of all the treated samples contained packets and blocks of well-refined lath-shaped martensite and retained austenite phases with varying grain sizes (2.8–7.9 μm). Among all the tested samples, TMCT-3 sample offered an optimum combination of properties by showing an improvement of 40% in tensile strength and reduced 34% elongation compared with the non-treated sample. Nanoindentation results were in good agreement with mechanical tests as the TMCT-3 sample exhibited a 51% improvement in indentation hardness with almost identical reduced elastic modulus compared with the non-treated sample. The electrochemical properties were analyzed in 0.1 M $NaHCO_3$ solution by potentiodynamic polarization and electrochemical impedance spectroscopy. As a result of TMCT, the minimum corrosion rate was 0.272 mm/a, which was twenty times less than that of the non-treated sample. The impedance results showed the barrier film mechanism, which was confirmed by the polarization results as the current density decreased.

Keywords: thermomechanical treatment; cyclic heat-treatment; nanoindentation; potentiodynamic polarization; electrochemical impedance spectroscopy

1. Introduction

Several industrial applications, particularly automotive industries, are demanding economical steels with superior strength, ductility, and impact toughness to manufacture lightweight structural components [1–4]. These properties can be achieved by producing stable and ultrafine grained microstructures [5]. For this purpose, several techniques, i.e., microalloying (of cobalt, copper, and boron in steel composition) [6], oxide dispersion strengthening technique [7–8], high-pressure torsion, equal channel angular pressing, accumulative roll bonding [5,9], controlling initial microstructure, austenitizing temperature, and austenitizing time [10], thermomechanical treatment (TMT) [11], and cyclic heat treatments [12], have been reported.

TMT is a well-recognized, economical, and efficient method of stabilizing and refining microstructure through bulk recrystallization of nanoscale $M_{23}C_6$ and MX-type carbide/carbonitride particles and nano sized subgrain boundaries in the matrix [7–8,13]. TMT has become the focal point for producing high-strength steels without alteration in composition in the last few years. In TMT, steel is heated to a sufficiently high temperature of about 1100°C, hot rolled into bars or rods, and quenched to room temperature [14]. The final microstructure, obtained after TMT, comprises refined martensite, retained austenite, and nanoscale carbide/carbonitride particles, resulting in significantly improved mechanical properties [15].

Cyclic heat treatment is also well-known economical method used for microstructural refinement [16]. Cyclic heat treatment involves repetition of austenitization [17–20], annealing [21], quenching [22], and tempering [23] processes. Several steels such as 9CrWVTiN steel [23], 5Cr steel [10], AISI 4140 steel [12], SCRAM steel [24], 16Cr–2Ni steel [17], high carbon-bearing steel [22], 0.34C-containing low-alloy Ni–Cr–Mo–V steel [18], P92 steel [19], and AISI D2 tool steel [20] have been investigated under cyclic heat treatment. Thus, significantly refined microstructure and im-

Corresponding author: Ameeq Farooq E-mail: ameeq.farooq@gmail.com

proved mechanical properties have been achieved. However, AISI 1345 steel has not been investigated under thermomechanical or cyclic heat treatments. AISI 1345 steel is one of the well-known steels used in manufacturing bolts and wear rings for different applications [5].

Bicarbonates are electroactive species that exist in the atmosphere, water, oil, and gas in small amounts and interact with metallic structures through both anodic and cathodic reactions. Corrosion of the steel structure in the bicarbonate environment is a substantial issue [25–26]. In industrial practice, several failures due to bicarbonate-induced corrosion have been reported [27–28]. Previous research described scale formation in the presence of bicarbonates on bare steel surface [29–32]. Wang and Atrens [33] explained the stress corrosion cracking mechanism in steel due to carbonate/bicarbonate ions and high pH electrolyte. Oskuie *et al.* [34] suggested that the critical current density during active to passive transition in carbonate/bicarbonate electrolyte indicates the initiation of stress corrosion cracking. Most of the previous researches were carried out on API X-series, i.e., X-65, X-70, X-80, and X-100, in near neutral and high pH carbonate/bicarbonate solutions [24,35–37]. In the present work, combinations of thermomechanical treatments and cyclic heat treatments were applied on AISI 1345 steel, and their effects on microstructure, mechanical, and electrochemical properties were investigated.

2. Experimental

2.1. Production of steel

AISI 1345 steel was cast on the laboratory scale in rod form. The chemical composition of the cast steel is given in Table 1.

Table 1. Chemical composition of AISI 1345 steel wt%

C	Si	Mn	S	P	Fe
0.45	0.37	1.78	0.017	0.002	Balance

2.2. Thermomechanical cyclic heat treatments

In thermomechanical cyclic heat treatment (TMCT), AISI 1345 cast steel rods were first heated to 1050°C for 120 min and then subjected to the rolling process. These rods were rolled into sheets of 5 mm thickness through multiple passes, followed by oil quenching. After rolling, sheets were subjected to three types of cyclic heat treatments (TMCT-1, TMCT-2, and TMCT-3), as illustrated in Fig. 1. In TMCT-1, steel was austenitized at 900°C for 30 min, oil quenched to room temperature, low-temperature tempered at 200°C for 60 min, and air-cooled to room temperature. This steel was then re-austenitized at 900°C for 30 min, oil quenched to room temperature, high-temperature tempered at 550°C for 60 min,

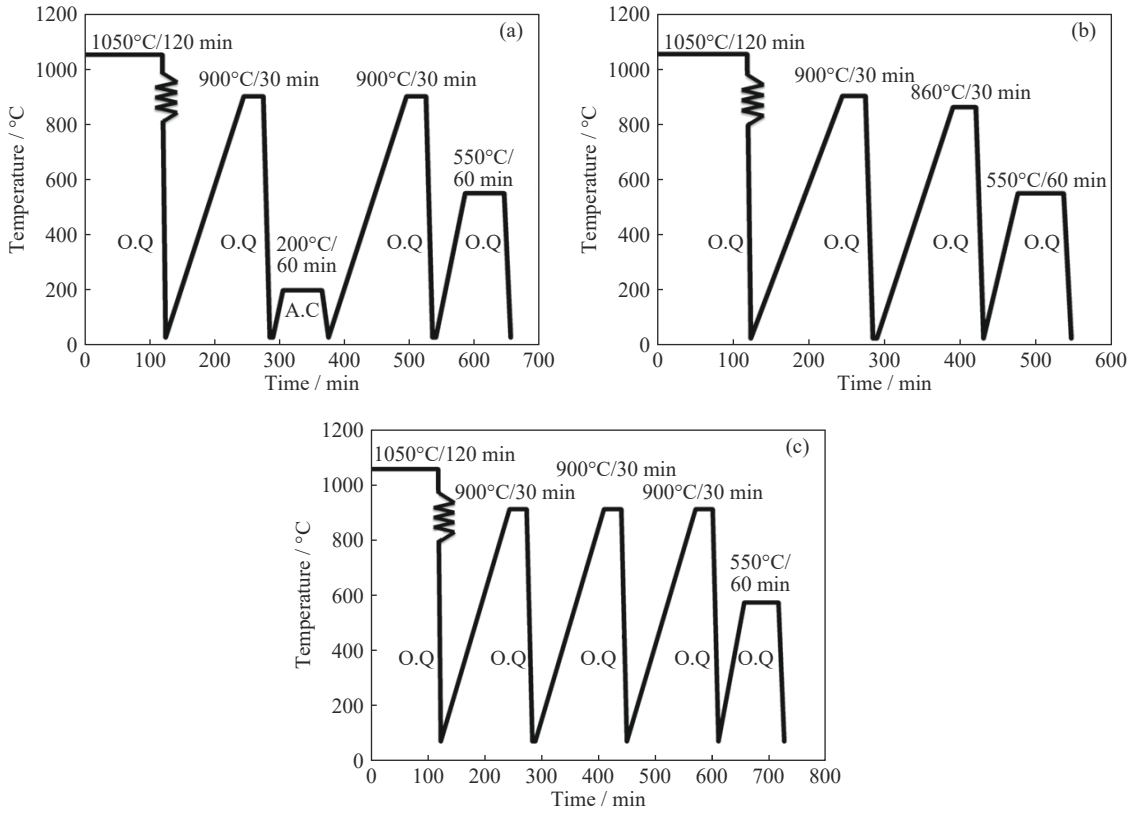

Fig. 1. Thermomechanical cyclic heat treatments applied to AISI 1345 steels: (a) TMCT-1; (b) TMCT-2; (c) TMCT-3 (O.Q—Oil quenching; A.C—Air cooling).

and oil quenched to room temperature. In TMCT-2, steel was first austenitized at 900°C for 30 min, oil quenched to room temperature, re-austenitized at a relatively lower temperature of 860°C for 30 min, oil quenched to room temperature, high-temperature tempered at 550°C for 60 min, and oil quenched to room temperature. In TMCT-3, steel was subjected to a cycle of austenitization at 900°C for 30 min, oil quenching for three times, and a final high-temperature tempering at 550°C for 60 min, followed by oil quenching to room temperature. For the quenching process, martensite start temperature (M_S) was determined by the Nehernberg equation [38]:

$$M_S = 498.9 - 300W_C - 33.3W_{Mn} - 22.2W_{Cr} - 16.7W_{Ni} - 11.1(W_{Si} + W_{Mo}) \quad (1)$$

where W_C, W_{Mn}, W_{Cr}, W_{Ni}, W_{Si}, and W_{Mo} are the weight fractions of C, Mn, Cr, Ni, Si, and Mo, respectively.

2.3. Microstructure analysis

For metallography, TMCT sheets were wire cut into dimensions of 1 cm × 1 cm × 0.5 cm. All samples were manually ground on SiC grinding papers grades P100, P200, P400, P600, P800, and P1000, and then polished on an automatic polisher (Struers Tegrapol–15 Grinder/Polisher, USA) with nylon and velvet cloths by using diamond pastes of grades 6, 3, 1, and 0.25 μm. Samples were then etched in 3vol% nital solution for 15 s. Microstructure was analyzed on an optical microscope (Leica Model DM-15000M, Germany) at 500× and scanning electron microscope (SEM, FEI brand model Inspect S50) at 2500× magnification. Grain size analysis was also carried out on the 100× magnification optical micrographs according to the ASTM E-112 standard.

2.4. Mechanical testing

To evaluate the effect of TMCT on the mechanical properties of AISI 1345 steel, hardness and tensile tests were performed. Rockwell hardness testing was carried out using a Rockwell hardness tester (Insize ISH-R150, China) with a diamond indenter and 980.67 N load. Five readings were taken and averaged to obtain the final value for each sample. For tensile testing, samples were machined and tested according to the ASTM E-8 standard.

2.5. Nanoindentation analysis

Nanoindentation analysis was also performed using a nanoindentation tester (CSM-international NHTX S/N: 01-2569, USA) to evaluate the micromechanical properties of AISI 1345 steel after TMCT. Tests were carried out in load control mode at a uniform loading/unloading rate of 200 mN/min up to a maximum load of 100 mN with a three-sided pyramidal diamond tip (Berkovich BJ-48, USA) having a nominal angle of 65.3° and diameter of 200 nm. For *in-situ* examination of the multiphase microstructure during analysis, a scanning probe microscope attached with a nanoindentation tester was used. For each sample, three readings were measured and averaged to obtain the final value.

2.6. Electrochemical analysis

Electrochemical properties of TMCT steels were investigated in 0.1 M $NaHCO_3$ solution. Samples were mounted on a specially designed copper sample holder using epoxy resin exposing one side (1 cm^2) to the electrolyte. Corrosion kinetics, mechanism, and polarization behavior of TMCT samples were analyzed at 35°C on potentiostat (Gamry Interface 1000, USA). Ag/AgCl electrode (with saturated KCl electrolyte) was used as reference, while graphite rod and TMCT samples were used as counter and working electrodes, respectively, in a three-electrode cell system by maintaining distance (~1 mm) between working and reference electrode using luggage probe to avoid short circuit. Open circuit potential (OCP) was run for 1 h to stabilize the potential and maintain the equilibrium between working electrode and electrolyte. Electrochemical impedance spectroscopy (EIS) was obtained at ±5 mV effective AC potential amplitude versus OCP in a frequency range of 100 kHz to 10 mHz. Potentiodynamic polarization curves were obtained by polarizing the working electrode in a potential range of 500–1500 mV versus OCP at a scan rate of 5 $mV \cdot s^{-1}$.

3. Results and discussion

3.1. Microstructure analysis

Macroscopic grain structures of all the non-treated and TMCT AISI 1345 steel samples are schematically presented in Fig. 2. From Fig. 2, the microstructures of AISI 1345 steels were significantly altered after TMCTs. Optical and SEM micrographs of all the samples are illustrated in Figs. 3 and 4, whereas the corresponding grain sizes are plotted in Fig. 5.

In the non-treated form, AISI 1345 steel possessed a coarse-grained (31.8 μm) microstructure that comprised a lamellar pearlite (P) phase and body-centered cubic (bcc) ferrite (α) phase (Figs. 3(a) and 3(b)). Pearlite phase was observed to be non-homogeneously segregated in the matrix of the ferrite phase. In TMCT, TMT treatment involved hot rolling, compressing the grains of all treated samples equally, and reducing the intergranular spacing. Subsequent cyclic heat treatments refined the grain sizes through microstructural phase transformation, as schematically presented in Fig. 2.

In the TMCT-1 sample, due to intermediate low-temperature tempering at 200°C in the first stage, nucleation of fine carbides in the matrix of martensite occurred, which provided preferential sites for nucleation and growth and refined the austenite phase during re-austenitization in the second stage. The grain size of martensite after re-quenching is directly proportional to the grain size of austenite before quenching [2–4,12]. Therefore, after TMCT-1, a grain refined (7.9 μm) microstructure comprising packets of martensite was ob-

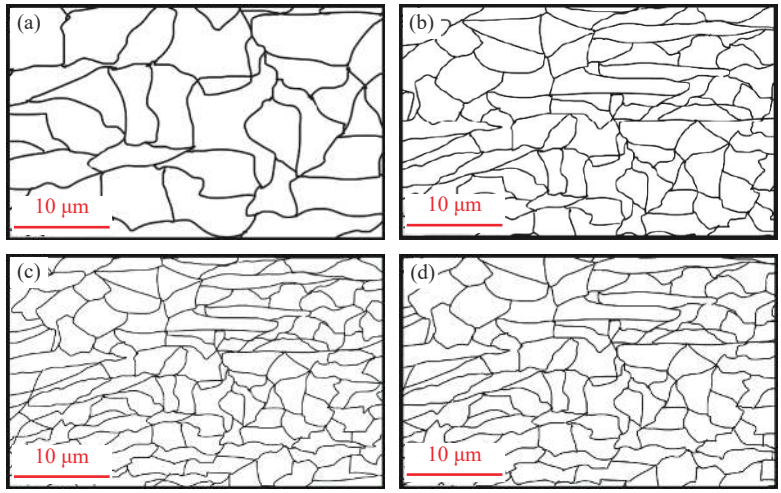

Fig. 2. Schematics of macroscopic grain structures of (a) non-treated, (b) TMCT-1, (c) TMCT-2, and (d) TMCT-3 AISI 1345 steels.

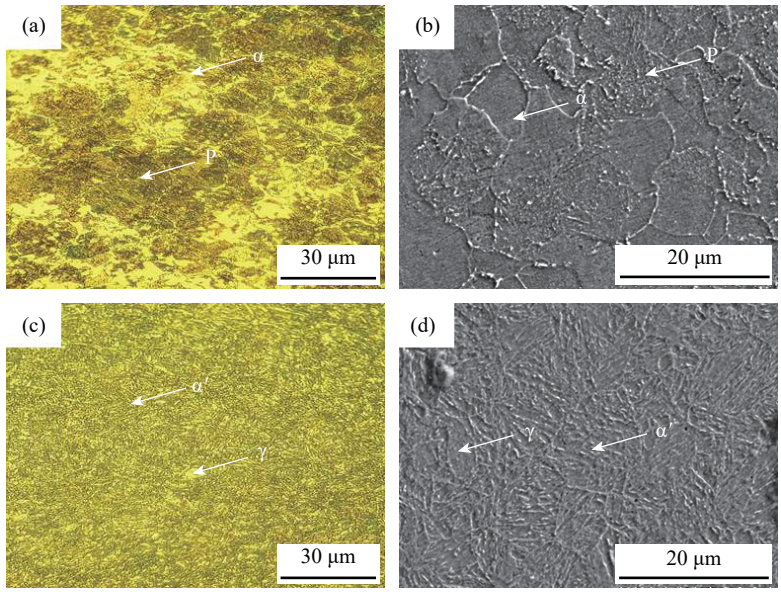

Fig. 3. Microstructures of (a, b) non-treated and (c, d) TMCT-1 AISI 1345 steel samples: (a, c) optical micrographs; (b, d) SEM micrographs.

tained. These packets contained blocks with the multi-variant crystallographic orientation, and the blocks consisted of laths of martensite. As a sufficient content of manganese (1.78wt%), as an austenite stabilizer, is present in the AISI 1345 steel, some fractions of austenite (γ) were retained after TMCT-1, as illustrated in Figs. 3(c) and 3(d); this result was similar to the findings reported by Sanij *et al.* [12].

In the TMCT-2 sample, the first austenitization at high temperature (900°C) dissolved an amount of coarse carbides and produced coarse microstructures after the first quenching. For grain refinement, re-austenitization at a relatively lower temperature (860°C) was performed after the first quenching. Re-austenitization followed by re-quenching can produce a highly homogeneous and refined grained microstructure that possesses increased volume fraction of retained austenite [10,24]. Therefore, in the current work, after TMCT-2, a highly refined grained (2.8 μm) microstructure was obtained. This microstructure comprised packets and blocks of martensite with increased volume fraction of retained austenite (Figs. 4(a) and 4(b)).

In TMCT-3, the purpose of repeating austenitization at the same temperature and oil quenching two times was to fully eliminate carbides and refine the microstructure. Therefore, the microstructure of TMCT-3 sample (5.6 μm) was refined than that of TMCT-1 sample but coarsened than that of TMCT-2 sample, containing the same aforementioned phases (Figs. 4(c) and 4(d)).

3.2. Mechanical properties

Microstructural grain refinement has a significant impact on the mechanical properties of polycrystalline metals [38–39]. Mechanical properties, i.e., tensile strength (TS),

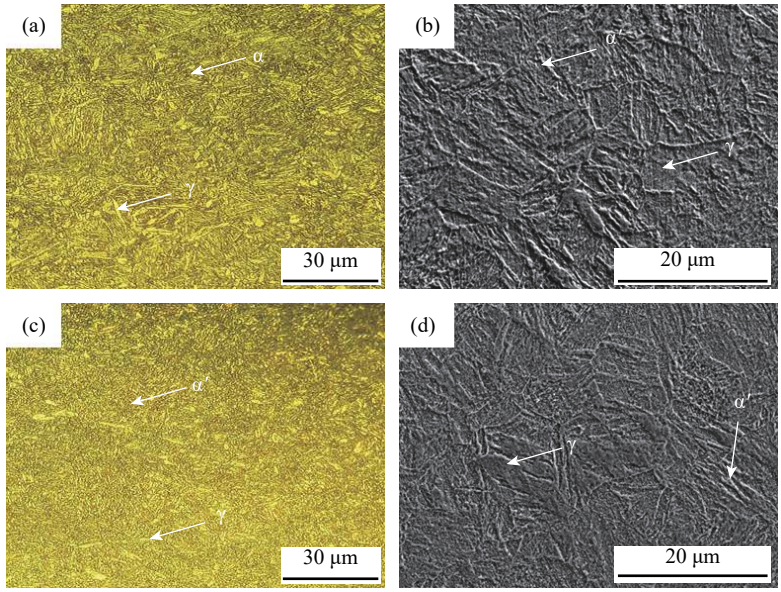

Fig. 4. Microstructures of (a, b) TMCT-2 and (c, d) TMCT-3 AISI 1345 steel samples: (a, c) optical micrographs; (b, d) SEM micrographs.

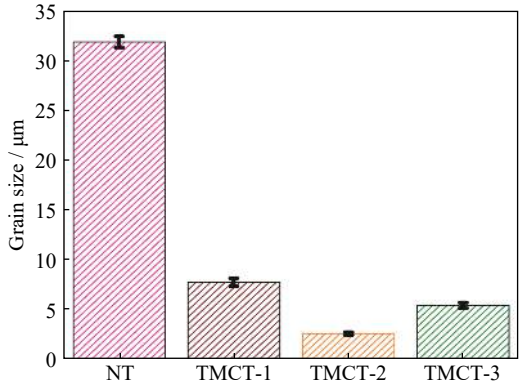

Fig. 5. Plot of grain sizes of the microstructures of non-treated (NT) and TMCT AISI 1345 steels.

yield strength ($YS_{0.2}$), elongation (ε_T), reduction in area (R_A), and calculated TS × ε_T factor of non-treated and TMCT AISI 1345 steels are given in Table 2. In the non-treated form, AISI 1345 steel exhibited a low TS (1090 MPa) and significantly high elongation (29%). These results could be attributed to the bcc ferrite and lamellar pearlite phases in the microstructure of non-treated AISI 1345 steel. The bcc ferrite phase is softer in nature and always offers low mechanical properties, whereas pearlite is lamellar structure of ferrite and cementite phases and offers relatively better but still lower mechanical properties than the bcc ferrite phase. In quenched and tempered steels, strengthening can be improved according to several mechanisms such as martensitic strengthening, precipitation strengthening, solid solution strengthening, dislocation strengthening, and grain size reduction strengthening [40–43]. In the current work, all the TMCTs caused grain refinement of microstructure. Therefore, martensitic strengthening and grain size reduction strengthening occurred in this work, similar to the literatures [44–48].

Table 2. Mechanical properties of the non-treated (NT) and TMCT AISI 1345 steels

Sample	TS / MPa	$YS_{0.2}$ / MPa	ε_T / %	R_A / %	(TS × ε_T) / (GPa·%)
NT	1090	919	29	19	31.61
TMCT-1	1395	1261	26	47	36.27
TMCT-2	1683	1560	16	35	26.93
TMCT-3	1529	1390	19	41	29.05

The TMCT-1 sample exhibited a 28% improvement in TS (1395 MPa) and 10% reduction in elongation (26%), compared with the non-treated sample. These changes were attributed to the formation of supersaturated lath martensite and retained austenite phases and fourfold refinement of these phases after TMCT-1 compared with the non-treated steel. Formation of the lath martensite phase increased the dislocation density of the steel and made it harder and stronger. By contrast, formation of the retained austenite improved the toughness of steel [49]. Refined grains have different crystallographic orientations and common grain boundaries. During plastic deformation, a moving dislocation needs to change the direction of motion while crossing the grain boundary. A dislocation cannot easily change the direction of motion due to significant crystallographic misorientations, resulting in strengthened steel. Another reason for strengthening of steel by grain size reduction is atomic disorder across the grain boundary, which creates discontinuity of slip planes [42–43], as illustrated in Fig. 6.

TMCT-2 sample demonstrated a 54.4% improvement in TS (1638 MPa) but a 44.8% reduction in elongation (16%), compared with the non-treated sample. These results were at-

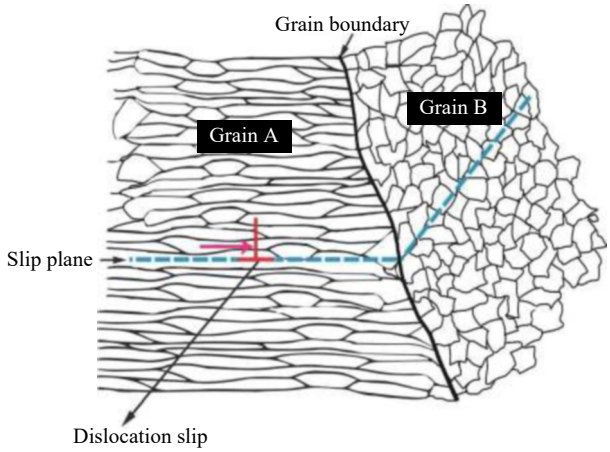

Fig. 6. Schematic of strengthening by grain size reduction occurred in the TMCT-1 AISI 1345 steel.

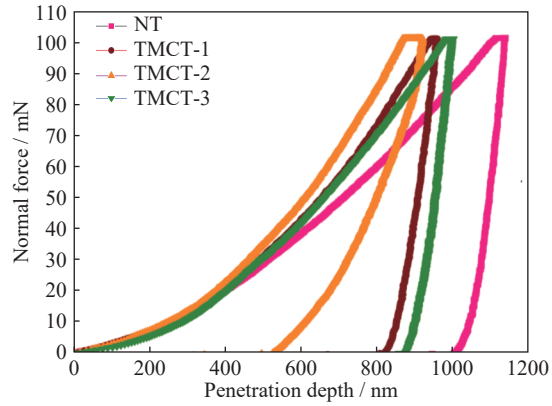

Fig. 7. Normal force–penetration depth curves of the non-treated (NT) and TMCT AISI 1345 steels obtained by nanoindentation analyses.

tributed to the 11-fold grain refinement of the microstructure, which comprised lath martensite and retained austenite phases that were obtained after TMCT-2, similar to the work of Rao and Thomas [50]. In TMCT-2, high-temperature austenitization and relatively lower temperature re-austenitization led to a well-refined microstructure with increased fractions of retained austenite, resulting in strengthening of steel. Double austenitization also reduces the intensity of temper embrittlement of steels [10].

TMCT-3 sample caused moderate 40% improvement in tensile strength (1529 MPa) and 34% reduction in elongation (19%), compared with the non-treated sample, because TMCT-3 caused sixfold grain refinement of microstructure.

3.3. Micromechanical properties

To evaluate the micromechanical properties of the non-treated and TMCT AISI 1345 steels, nanoindentation analysis was performed. Normal force–penetration depth curves, obtained after nanoindentation analysis, are illustrated in Fig. 7. The corresponding measured quantities, i.e., indentation hardness (H), Vickers hardness (H_V), reduced elastic modulus (E_r), and stiffness (S), are given in Table 3. The indentation hardness (H) was calculated using Eq. (2) [51–52]:

$$H = \frac{P_{max}}{A} \tag{2}$$

where P_{max} is the applied load, and A is the projected contact area. Vickers hardness (H_V) was calculated using Eq. (3) [51–52]:

$$H_V = \frac{P_{max}}{A_D} \tag{3}$$

where A_D is the developed area. Reduced elastic modulus (E_r) was calculated using Eq. (4) [51–52]:

$$E_r = \frac{\sqrt{\pi}}{2}\frac{S}{\sqrt{A}} \tag{4}$$

where S is stiffness.

Table 3. Micromechanical properties of the non-treated (NT) and TMCT AISI 1345 steels

Sample	H / MPa	H_V, VHN	E_r / GPa	S / (mN·nm^{-1})
NT	3143	291	262	0.526
TMCT-1	4274	396	206	0.349
TMCT-2	6707	621	119	1.522
TMCT-3	4746	439	280	0.990

In non-treated form, AISI 1345 steel possessed low values of H (3143 MPa) and H_V (VHN 291) and moderate values of E_r (262 GPa) and S (0.526 mN/nm). These properties were attributed to the presence of bcc ferrite and lamellar structured pearlite phases in the microstructure. TMCT-1 sample exhibited a 36% improvement in H and H_V at the 21% expense of E_r and 34% expense of S, compared with the non-treated sample. This was due to the fourfold grain refinement in microstructure, having lath-shaped martensite and retained austenite phases produced by TMCT-1.

TMCT-2 produced 11-fold refinement and caused maximum strengthening of steel at a loss of elongation. Therefore, TMCT-2 sample exhibited a maximum twofold improvement in H and H_V, threefold improvement in S, and maximum twofold reduction in E_r, compared with the non-treated sample. Meanwhile, TMCT-3 produced sixfold refinement compared with the non-treated sample, thereby offering optimum balance in micromechanical properties. TMCT-3 sample demonstrated 51% improvement in H and H_V, 7% in E_r, and 88% in S. Micromechanical properties of TMCT AISI 1345 steels were in good agreement with the mechanical properties above.

3.4. Electrochemical properties

3.4.1. Open circuit potential

The OCPs of the non-treated and TMCT AISI 1345 steel samples, measured in 0.1 M $NaHCO_3$ solution at 35°C, are illustrated in Fig. 8.

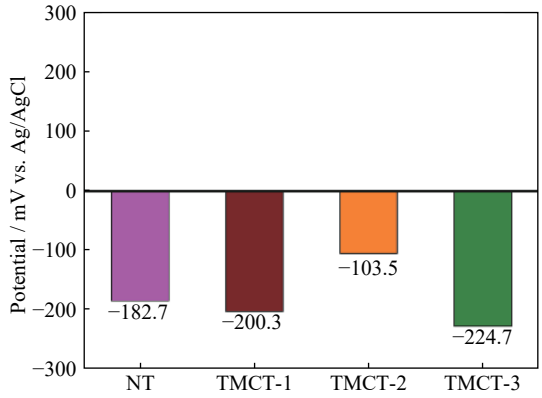

Fig. 8. Open circuit potentials of the non-treated and TMCT AISI 1345 steels.

Non-treated AISI 1345 steel showed a negative OCP of −182.7 mV vs. Ag/AgCl, and this value was attributed to its coarse-grained (31.6 μm) microstructure. For the TMCT-1 sample, it shifted toward a more negative (active) potential of −200.3 mV vs. Ag/AgCl due to the grain refined (7.9 μm) microstructure. For the TMCT-2 sample, a sharp shift in OCP was observed toward a positive (noble) direction at −103.5 mV vs. Ag/AgCl, because of the homogeneous and grain refined (2.8 μm) austenite phase. The OCP of the TMCT-3 sample drastically shifted toward a negative (active) direction at −224.7 mV vs. Ag/AgCl, because of grain coarsening (up to 5.6 μm) compared with the TMCT-2 sample. Moreover, the highly negative potential of the TMCT-3 sample in 0.1 M $NaHCO_3$ solution, referred to as the active state of the surface, presented its high tendency to react with the electrolyte.

3.4.2. Electrochemical impedance spectroscopy

EIS was performed to determine the corrosion mechanism of passive/barrier film growth on the non-treated and TMCT AISI 1345 steel samples in 0.1 M $NaHCO_3$ solution at 35°C in the frequency range of 100 kHz to 10 mHz with alternating voltage range of ±5 mV. Nyquist plots are illustrated in Fig. 9. Equivalent electrical circuits (EECs) used to fit the Nyquist plots are presented in Fig. 10, and the parameters calculated by Echem Analyst software are tabulated in Table 4. The electrochemical parameters in the EEC model are as follows: R_s is the solution/electrolyte resistance, R_{bf} is the barrier film resistance, R_{ct} is the charge transfer resistance, Y_{dl} is the non-ideal double layer capacitance, and Y_{bf} is the non-ideal barrier film capacitance. In the Bode plot, impedance modulus corresponding to high frequency is usually referred to as solution/electrolyte resistance; at low frequency, it usually corresponds to charge transfer resistance [53].

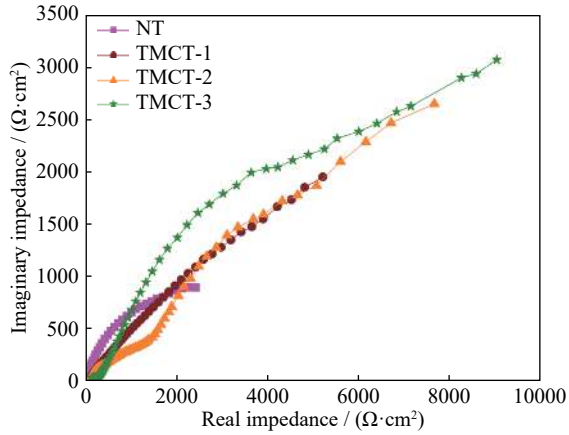

Fig. 9. Nyquistplot of the non-treated and TMCT AISI 1345 steels.

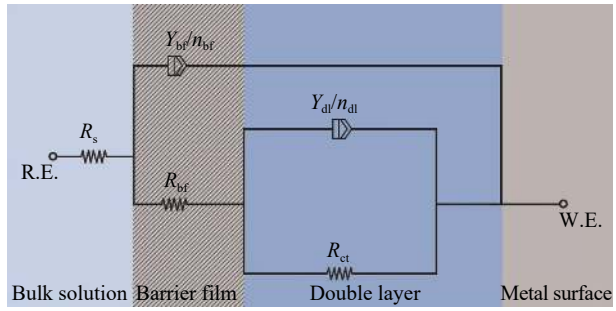

Fig. 10. Schematic representation of the simulated EEC model for AISI 1345 steel (R.E.—Reference electrode; W.E.—Working electrode; n_{bf}—Constant phase of barrier film; n_{dl}—Constant phase of double layer).

Table 4. Electrochemical parameters obtained from the EIS spectra of the non-treated and TMCT AISI 1345 steels

Sample	R_s / (Ω·cm²)	R_{bf} / (Ω·cm²)	Y_{bf} / (μF·cm^{-2})	n_{bf}	Y_{dl} / (μF·cm^{-2})	n_{dl}	R_{ct} / (kΩ·cm²)
NT	20.54	545	379.80	0.7255	702.2	0.3562	5.134
TMCT-1	50.73	1008	138.90	0.4456	292.7	0.3609	12.470
TMCT-2	69.77	1014	24.53	0.4944	341.5	0.4559	14.530
TMCT-3	15.91	402	37.75	0.3476	121.9	0.5409	12.470

The barrier film may develop on the steel surface due to the formation of iron carbonate or complex iron carbonates. The formation of a barrier film depends on the dissolution rate of steel, grain size, and microstructural phases [37]. R_{bf} for the non-treated steel sample was observed to be 545 Ω·cm². This finding was attributed to the coarse grained and non-homogenous microstructure of AISI 1345 steel in non-treated form. After TMCT-1, R_{bf} increased to 1008 Ω·cm² due to the substantially refined (7.9 μm) microstructure obtained. The refined microstructure increased the dissolution rate and formed a thick barrier film, which resisted the current flow. The R_{bf} value further increased to 1014 Ω·cm² after

TMCT-2 due to further refinement of microstructural grains. However, after TMCT-3, R_{bf} decreased to 402 Ω·cm^2. This change might be associated with the formation of moderately refined and stable retained austenite martensite phases after TMCT-3, which retarded the formation mechanism of the barrier film. Compared with the non-treated samples, both TMCT-1 and TMCT-3 increased R_{ct} to 12.47 kΩ·cm^2, whereas TMCT-2 further increased it to 14.53 kΩ·cm^2.

3.4.3. Potentiodynamic polarization

The effect of TMCT on the corrosion tendency of AISI 1345 steel was estimated from the potentiodynamic polarization curves in 0.1 M $NaHCO_3$ solution at 35°C (Fig. 11). The potentiodynamic polarization curves presented the active/passive behaviors of the non-treated and TMCT AISI 1345 steels. These curves were then Tafel fitted using Echem Analyst software, and the values are tabulated in Table 5.

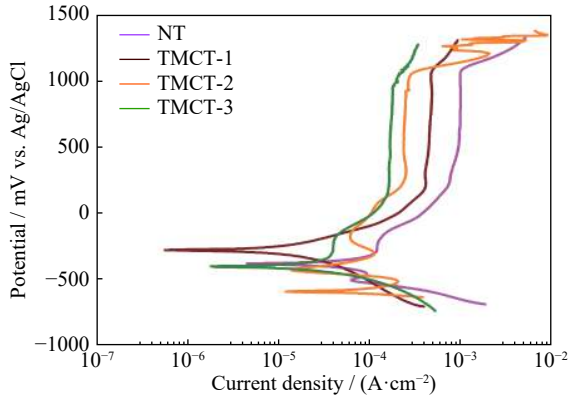

Fig. 11. Potentiodynamic polarization curves of the non-treated and TMCT AISI 1345 steels.

Table 5. Electrochemical parameters calculated from potentiodynamic polarization curves of AISI 1345 steels

Sample	i_{corr} / (μA·cm^{-2})	E_{corr} / mV	Corrosion rate / (mm·a^{-1})	E_{bd} / mV	i_p / (μA·cm^{-2})
NT	604.0	−380	7.026	1082.0	1049.0
TMCT-1	23.4	−273	0.272	1069.0	495.6
TMCT-2	189.0	−587	2.196	1032.0	260.6
TMCT-3	91.3	−400	1.061	952.5	181.7

Under applied conditions, $NaHCO_3$ could separate into sodium ion (Na^+) and bicarbonate ions (HCO_3^-). During cathodic polarization, bicarbonates may dilute to carbonates with the evolution of hydrogen gas (H_2) according to reactions (5) and (6) [35]:

$$HCO_3^- + e^- \rightarrow H_{ad.} + CO_3^{2-} \quad (5)$$

$$HCO_3^- + e^- + H_{ad.} \rightarrow H_2 + CO_3^{2-} \quad (6)$$

The cathodic polarization curves of all the TMCT samples were the same. However, for the non-treated sample, the cathodic reaction was disturbed and a small kink was formed due to reaction (5) and formation of adsorbed hydrogen ($H_{ad.}$).

Non-treated steel sample showed a corrosion rate of 7.026 mm/a and a corrosion current density (i_{corr}) of 604 μA·cm^{-2}. The negative corrosion potential (E_{corr}) value of −380 mV of the non-treated sample was associated with the presence of non-homogeneously segregated lamellar pearlite phase in the matrix of the bcc ferrite phase. During anodic polarization, iron (Fe) may dissolve in the activation polarization region when the corrosion current density reached 127 μA·cm^{-2} and potential of −293 mV. The current density became constant, which indicated barrier/passive film formation on the steel surface due to the following reaction (7) [54]:

$$Fe + 2H_2O \rightarrow Fe(OH)_2 + 2H^+ + 2e^- \quad (7)$$

The above reaction is a complex reaction and takes place step-by-step as represented in reactions (8)–(11) due to the formation and adsorption of intermediate species (i.e., adsorbed $FeOH^-$ ($FeOH^-_{ads}$), adsorbed FeOH ($FeOH_{ads}$), and adsorbed $FeOH^+$ ($FeOH^+_{ads}$)) at the steel surface.

$$Fe + OH^- \rightarrow FeOH^-_{ads} \quad (8)$$

$$FeOH^-_{ads} \rightarrow FeOH_{ads} + e^- \quad (9)$$

$$FeOH_{ads} \rightarrow FeOH^+_{ads} + e^- \quad (10)$$

$$FeOH^+_{ads} + OH^- \rightarrow Fe(OH)_2 \quad (11)$$

The barrier film that formed on the non-treated steel surface broke down at the potential above −293 mV, and the dissolution of steel began. When the potential reached 487 mV, the barrier film formed again, which was most probably due to the corrosion product formed on the steel surface. According to previous research [55], the complex iron hydroxyl carbonate ($Fe_2(OH)_2CO_3$) species formed on the steel surface, which was exposed to the electrolyte as reaction (12):

$$2Fe + HCO_3^- + 2H_2O \rightarrow Fe_2(OH)_2CO_3 + 3H^+ + 4e^- \quad (12)$$

The formed species may react further with HCO_3^- species, and $FeCO_3$ formed according to reaction (13):

$$Fe_2(OH)_2CO_3 + HCO_3^- + H^+ \rightarrow 2FeCO_3 + 2H_2O \quad (13)$$

The barrier film formed at a constant current density of 1.04 mA·cm^{-2} called passive current density (i_p), which further stopped the dissolution reaction. When the potential further increased, the current density remained constant at the potential range of 487–622 mV. Subsequently, the barrier film broke down at the breakdown potential (E_{bd}) of 1082 mV. At this high potential, iron carbonate ($FeCO_3$) could react with dissolved bicarbonate ions and form soluble ferrous carbonate complex $Fe(CO_3)_2^{2-}$ according to reaction (14):

$$FeCO_3 + HCO_3^- \rightarrow Fe(CO_3)_2^{2-} + H^+ \quad (14)$$

After TMCT-1, the corrosion rate decreased to 0.272 mm/a due to its corrosion current density decreasing to 23.40 μA·cm^{-2}, compared with the non-treated sample. Moreover, its less negative E_{corr} value of −273 mV corresponded to the nucleation of fine carbides in the martensitic matrix, which provided preferential sites for nucleation, growth, and refinement of austenite during re-austenitization. The anodic polarization curve of the TMCT-1 sample showed that there was no barrier film of the iron hydroxide layer ($Fe(OH)_2$) formed at low potential, which was formed in the non-treated steel sample. At the potential of 201.4 mV and current density of 448.5 μA·cm^{-2}, the iron hydroxide layer formed, which was unstable at high potential and may breakdown in the presence of bicarbonates according to reaction (15) and formed another barrier film of iron carbonate [55]:

$$Fe(OH)_2 + HCO_3^- \rightarrow FeCO_3 + H_2O + OH^- \quad (15)$$

The i_p value (495.6 μA·cm^{-2}) for TMCT-1 sample was very small, compared with that of non-treated steel sample, which indicated that the TMCT-1 sample had low dissolution and formed a barrier film at low current density. With further increase in the potential, the current density remained constant at the potential range of 201.4–1036.4 mV, which was wider compared with that of the non-treated sample, and the barrier film broke down at E_{bd} of 1069 mV.

By contrast, the TMCT-2 sample formed two active–passive nose sat low and high potentials. The first active–passive nose was formed at the critical current density (i_{cc1}) of 219.1 μA·cm^{-2}, which corresponded to the potential (E_{cc1}) of −519.4 mV. This first nose formation was attributed to its refined grained microstructure compared with the other samples. The mass transfer-controlled electrochemical process was mostly related to the surface coverage by $Fe(OH)_2$ (reaction (7)). As the formation of $Fe(OH)_2$ is a stepwise reaction, the anodic polarization curve moved toward the low current density value and underwent active to passive transition. Upon reaching the low current density of 14.31 μA·cm^{-2} and potential of −424.8 mV, the current density abruptly changed and stopped the formation of $Fe(OH)_2$. The second active–passive nose formed at the critical current density (i_{cc2}) of 120.1 μA·cm^{-2}, which corresponded to the potential (E_{cc2}) of −301.5 mV due to the formation of complex iron hydroxyl carbonate $Fe_2(OH)_2CO_3$ species on the steel surface according to reaction (12). When the potential increased to 288.8 mV, the barrier film of $FeCO_3$ formed at i_p of 260.6 μA·cm^{-2} and broke at E_{bd} of 1032 mV. As a result of the refined grained microstructure and increased fractions of retained austenite, the TMCT-2 sample exhibited a corrosion rate of 2.196 mm/a, corrosion current density of 189 μA·cm^{-2}, and passivation range of 288.8–1171.1 mV.

For the TMCT-3 sample, the corrosion rate decreased (1.061 mm/a) again with the decrease in the corrosion current density (91.30 μA·cm^{-2}) as compared to the TMCT-2 sample. The E_{corr} value of −400 mV corresponded to its refined grains as compared with that of TMCT-1 steel due to rapid cycles of quenching. The i_p value of 181.7 μA·cm^{-2} was less than that of all the samples, and the E_{bd} value was 952.5 mV, which was almost at the same potential as those of the other heat-treated samples.

4. Conclusions

The following conclusions were drawn from this work:

(1) A well-refined microstructure, comprising packets and blocks of lath-shaped martensite and retained austenite, was achieved by all the TMCT methods. TMCT-2 offered maximum grain refinement (from 31.8 to 2.8 μm) among all treatments.

(2) Among all the TMCT methods, the maximum TS (1683 MPa) was achieved after TMCT-2 with minimum ε_T value, whereas the maximum value of ε_T (26%) was achieved after TMCT-1 with minimum TS. TMCT-3 provided an optimum combination of TS (1529 MPa) and ε_T (19%).

(3) The maximum values of H (6707 MPa), H_V (VHN 621), and S (1.522 mN/nm) and minimum value of E_r (119 GPa) were achieved after TMCT-2. However, TMCT-3 offered an optimum combination of H (4746 MPa), H_V (VHN 439), and S (0.990 mN/nm), with a maximum value of E_r (280 GPa).

(4) TMCT methods substantially improved the corrosion resistance of AISI 1345 steel. TMCT-1 caused the maximum reduction in the corrosion rate from 7.026 to 0.272 mm/a and altered the mechanism of the formation of barrier film on the steel surface by decreasing the passive current from 1049 to 495.6 μA·cm^{-2}, as compared to the non-treated steel.

References

[1] Y. Tomita, Development of fracture toughness of ultrahigh strength, medium carbon, low alloy steels for aerospace applications, *Int. Mater. Rev.*, 45(2000), No. 1, p. 27.

[2] Y. Tomita and K. Okabayashi, Modified heat treatment for lower temperature improvement of the mechanical properties of two ultrahigh strength low alloy steels, *Metall. Trans. A*, 16(1985), No. 1, p. 83.

[3] Y.Q. Weng, *Ultra-Fine Grained Steels*, Metallurgical Industry Press, Beijing and Springer, Berlin, Heidelberg, 2009, p. 300.

[4] S. Kim, S. Lee, and B.S. Lee, Effects of grain size on fracture toughness in transition temperature region of Mn–Mo–Ni low-alloy steels, *Mater. Sci. Eng. A*, 359(2003), No. 1-2, p. 198.

[5] M. Eskandari, A. Kermanpur, and A. Najafizadeh, Formation of nano-grained structure in a 301 stainless steel using a repetitive thermo-mechanical treatment, *Mater. Lett.*, 63(2009), No. 16, p. 1442.

[6] P. Prakash, J. Vanaja, N. Srinivasan, P. Parameswaran, G.V.S.N. Rao, and K. Laha, Effect of thermo-mechanical treatment on tensile properties of reduced activation ferritic-martensitic steel, *Mater. Sci. Eng. A*, 724(2018), p. 171.

[7] S.Z. Li, Z. Eliniyaz, F. Sun, Y.Z. Shen, L.T. Zhang, and A.D. Shan, Effect of thermo-mechanical treatment on microstructure and mechanical properties of P92 heat resistant steel, *Mater. Sci. Eng. A*, 559(2013), p. 882.

[8] H. Oka, T. Tanno, S. Ohtsuka, Y. Yano, T. Uwaba, T. Kaito, and M. Ohnuma, Effect of thermo-mechanical treatments on nano-structure of 9Cr-ODS steel, *Nucl. Mater. Energy*, 9(2016), p. 346.

[9] C.Y. Lee, C.S. Yoo, A. Kermanpur, and Y.K. Lee, The effects of multi-cyclic thermo-mechanical treatment on the grain refinement and tensile properties of a metastable austenitic steel, *J. Alloys Compd.*, 583(2014), p. 357.

[10] J. Liu, H. Yu, T. Zhou, C.H. Song, and K. Zhang, Effect of double quenching and tempering heat treatment on the microstructure and mechanical properties of a novel 5Cr steel processed by electro-slag casting, *Mater. Sci. Eng. A*, 619(2014), p. 212.

[11] P. Prakash, J. Vanaja, D.P.R. Palaparti, G.V.P. Reddy, K. Laha, and G.V.S.N. Rao, Tensile flow and work hardening behavior of reduced activation ferritic martensitic steel subjected to thermo-mechanical treatment, *J. Nucl. Mater.*, 520(2019), p. 19.

[12] M.H.K. Sanij, S.S.G. Banadkouki, A.R. Mashreghi, and M. Moshrefifar, The effect of single and double quenching and tempering heat treatments on the microstructure and mechanical properties of AISI 4140 steel, *Mater. Des.*, 42(2012), p. 339.

[13] P. Ganesh, A.V. Kumar, C. Thinaharan, N.G. Krishna, R.P. George, N. Parvathavarthini, S.K. Rai, R. Kaul, U.K. Mudali, and L.M. Kukreja, Enhancement of intergranular corrosion resistance of type 304 stainless steel through a novel surface thermo-mechanical treatment, *Surf. Coat. Technol.*, 232(2013), p. 920.

[14] A. Ghosh and M. Ghosh, Tensile and impact behaviour of thermo mechanically treated and micro-alloyed medium carbon steel bar, *Constr. Build. Mater.*, 192(2018), p. 657.

[15] L. Kučerová and M. Bystrianský, Comparison of thermo-mechanical treatment of C–Mn–Si–Nb and C–Mn–Si–Al–Nb TRIP steels, *Procedia Eng.*, 207(2017), p. 1856.

[16] M.A. Hafeez, A. Inam, and A. Farooq, Mechanical and corrosion properties of medium carbon low alloy steel after cyclic quenching and tempering heat-treatments, *Mater. Res. Express*, 7(2020), No. 1, art. No. 016553.

[17] K.P. Balan, A.V. Reddy, and D.S. Sarma, Effect of single and double austenitization treatments on the microstructure and mechanical properties of 16Cr–2Ni Steel, *J. Mater. Eng. Perform.*, 8(1999), No. 3, p. 385.

[18] E. Chang, C.Y. Chang, and C.D. Liu, The effects of double austenitization on the mechanical properties of a 0.34C containing low-alloy Ni–Cr–Mo–V steel, *Metall. Mater. Trans. A*, 25(1994), No. 3, p. 545.

[19] C. Pandey, M.M. Mahapatra, P. Kumar, P. Kumar, N. Saini, J.G. Thakare, and S. Kumar, Study on effect of double austenitization treatment on fracture morphology tensile tested nuclear grade P92 steel, *Eng. Fail. Anal.*, 96(2019), p. 158.

[20] S. Salunkhe, D. Fabijanic, J. Nayak, and P. Hodgson, Effect of single and double austenitization treatments on the microstructure and hardness of AISI D2 tool steel, *Mater. Today: Proc.*, 2(2015), No. 4-5, p. 1901.

[21] M.A. Hafeez, A. Inam, M.U. Hassan, M.A. Umer, M. Usman, and A. Hanif, Optimized corrosion performance of AISI 1345 steel in hydrochloric acid through thermos-mechanical cyclic annealing processes, *Crystals*, 10(2020), No. 4, p. 265.

[22] Z.X. Cao, Z.Y. Shi, F. Yu, K. Sugimoto, W.Q. Cao, and Y.Q. Weng, Effects of double quenching on fatigue properties of high carbon bearing steel with extra-high purity, *Int. J. Fatigue*, 128(2019), art. No. 105176.

[23] Y. Zhang, C. Yu, T. Zhou, D.W. Liu, X.W. Fang, H.P. Li, and J.P. Suo, Effects of Ti and a twice-quenching treatment on the microstructure and ductile brittle transition temperature of 9CrWVTiN steels, *Mater. Des.*, 88(2015), p. 675.

[24] X.S. Xiong, F. Yang, X.R. Zou, and J.P. Suo, Effect of twice quenching and tempering on the mechanical properties and microstructures of SCRAM steel for fusion application, *J. Nucl. Mater.*, 430(2012), No. 1-3, p. 114.

[25] J.G. Gonzalez-Rodriguez, M. Casales, V.M. Salinas-Bravo, J.L. Albarran, and L. Martinez, Effect of microstructure on the stress corrosion cracking of X-80 pipeline steel in diluted sodium bicarbonate solutions, *Corrosion*, 58(2002), No. 7, p. 584.

[26] M.H. Nazari, S.R. Allahkaram, and M.B. Kermani, The effects of temperature and pH on the characteristics of corrosion product in CO_2 corrosion of grade X70 steel, *Mater. Des.*, 31(2010), No. 7, p. 3559.

[27] S.J. Harjac, A. Atrens, C.J. Moss, and V. Linton, Influence of solution chemistry and surface condition on the critical inhibitor concentration for solutions typical of hot potassium carbonate CO_2 removal plant, *J. Mater. Sci.*, 42(2007), No. 18, p. 7762.

[28] S. Nešić, Key issues related to modelling of internal corrosion of oil and gas pipelines–A review, *Corros. Sci.*, 49(2007), No. 12, p. 4308.

[29] F.M. Al-Kharafi, B.G. Ateya, and R.M. Abdallah, Electrochemical behaviour of low carbon steel in concentrated carbonate chloride brines, *J. Appl. Electrochem.*, 32(2002), No. 12, p. 1363.

[30] M. Attarchi, M. Mazloumi, S.K. Sadrnezhaad, A. Jafari, and M. Asadi, Formation and rupture of carbonate film: An electrochemical noise approach, *Anti-Corros. Methods Mater.*, 56(2009), No. 2, p. 103.

[31] S. Simard, H. Menard, and L. Brossard, Localized corrosion of 1024 mild steel in slightly alkaline bicarbonate solution with Cl^- ions, *J. Appl. Electrochem.*, 28(1998), No. 2, p. 151.

[32] S. Simard, M. Odziemkowski, D.E. Irish, L. Brossard, and H. Ménard, *In situ* micro-Raman spectroscopy to investigate pitting corrosion product of 1024 mild steel in phosphate and bicarbonate solutions containing chloride and sulfate ions, *J. Appl. Electrochem.*, 31(2001), No. 8, p. 913.

[33] J.Q. Wang and A. Atrens, SCC initiation for X65 pipeline steel in the "high" pH carbonate/bicarbonate solution, *Corros. Sci.*, 45(2003), No. 10, p. 2199.

[34] A.A. Oskuie, T. Shahrabi, A. Shahriari, and E. Saebnoori, Electrochemical impedance spectroscopy analysis of X70 pipeline steel stress corrosion cracking in high pH carbonate solution, *Corros. Sci.*, 61(2012), p. 111.

[35] F.F. Eliyan, E.S. Mahdi, and A. Alfantazi, Electrochemical evaluation of the corrosion behaviour of API-X100 pipeline steel in aerated bicarbonate solutions, *Corros. Sci.*, 58(2012), p. 181.

[36] J.B. Han, B.N. Brown, D. Young, and S. Nešić, Mesh-capped probe design for direct pH measurements at an actively corroding metal surface, *J. Appl. Electrochem.*, 40(2010), No. 3, p. 683.

[37] A. Farooq, A.A. Alvi, A.M.H. Alvi, K.M. Deen, and A. Tariq, Effect of post weld heat treatment on the electrochemical behavior of API X-65 welded pipeline in bicarbonates solutions, [in] *Conference Proceeding: NACE Northern Area Western Conference*, Calgary, Alberta, 2019, p. 683.

[38] A. Inam, Y. Imtiaz, M.A. Hafeez, S. Munir, Z. Ali, M. Ishtiaq,

M.H. Hassan, A. Maqbool, and W. Haider, Effect of tempering time on microstructure, mechanical, and electrochemical properties of quenched–partitioned–tempered advanced high strength steel (AHSS), *Mater. Res. Express*, 6(2019), art. No. 126509.

[39] M.A. Hafeez, Investigation on mechanical properties and immersion corrosion performance of 0.35%C–10.5%Mn steel processed by austenite reverted transformation (ART) annealing process, *Metall. Microstruct. Anal.*, 9(2020), p. 159.

[40] C. Liu, Z.B. Zhao, D.O. Northwood, and Y.X. Liu, A new empirical formula for the calculation of M_S temperatures in pure iron and super-low carbon alloy steels, *J. Mater. Process. Technol.*, 113(2001), No. 1-3, p. 556.

[41] Y.P. Zhang, D.P. Zhan, X.W. Qi, Z.H. Jiang, and H.S. Zhang, Microstructure and mechanical properties of Cr14 ultra-high-strength steel at different tempering temperatures around 773 K, *Mater. Sci. Eng. A*, 698(2017), p. 152.

[42] W.D. Callister Jr. and D.G. Rethwisch, *Material Science and Engineering: An Introduction*, 8th ed., John Wiley and Sons, New Jersey, Hoboken, 2009.

[43] G.E. Dieter, *Mechanical Metallurgy*, 3rd ed., McGraw-Hill-Book Co., New York, 1986.

[44] M.A. Hafeez and A. Farooq, Microstructural, mechanical and tribological investigation of 30CrMnSiNi2A ultra-high strength steel under various tempering temperatures, *Mater. Res. Express*, 5(2018), No. 1, art. No. 016505.

[45] M.A. Hafeez, Effect of microstructural transformation during tempering on mechanical properties of quenched and tempered 38CrSi steel, *Mater. Res. Express*, 6(2019), No. 8, art. No. 086552.

[46] M.A. Hafeez, A. Inam, and M.A. Arshad, Investigation on microstructural, mechanical, and electrochemical properties of water, brine quenched and tempered low carbon steel, *Mater. Res. Express*, 6(2019), No. 9, art. No. 096524.

[47] M.A. Hafeez and A. Farooq, Effect of heat treatments on the mechanical and electrochemical behavior of 38CrSi and AISI 4140 steels, *Metall. Microstruct. Anal.*, 8(2019), No. 4, p. 479.

[48] M.A. Hafeez and A. Farooq, Effect of quenching baths on microstructure and hardness of AISI1035 steel, *Niger. J. Technol. Res.*, 13(2018), No. 1, p. 82.

[49] M.A. Hafeez, M. Usman, M.A. Arshad, and M.A. Umer, Nanoindentation-based micro-mechanical and electrochemical properties of quench-hardened, tempered low-carbon steel, *Crystals*, 10(2020), No. 6, p. 508.

[50] B.V.N. Rao and G. Thomas, Structure-property relations and the design of Fe–4Cr–C base structural steels for high strength and toughness, *Metall. Trans. A*, 11(1980), p. 441.

[51] W.C. Oliver and G.M. Pharr, An improved technique for determining hardness and elastic modulus using load and displacement sensing indentation experiments, *J. Mater. Res.*, 7(1992), No. 6, p. 1564.

[52] G. Guillonneau, G. Kermouche, S. Bec, and J.-L. Loubet, Determination of mechanical properties by nanoindentation independently of indentation depth measurement, *J. Mater. Res.*, 27(2012), No. 19, p. 2551.

[53] L. Hao, S.X. Zhang, J.H. Dong, and W. Ke, Evolution of corrosion of MnCuP weathering steel submitted to wet/dry cyclic tests in a simulated coastal atmosphere, *Corros. Sci.*, 58(2012), p. 175.

[54] S.I. Hirnyi, Anodic hydrogenation of iron in a carbonate–bicarbonate solution, *Mater. Sci.*, 37(2001), No. 3, p. 491.

[55] D.H. Davies and G.T. Burstein, The effects of bicarbonate on the corrosion and passivation of iron, *Corrosion*, 36(1980), No. 8, p. 416.